Broadband Nonlinear Wavelength Conversion with Integrated Microresonators

Jennifer A. Black, Su-Peng Yu, Zachary L. Newman, David R. Carlson, Jizhao Zang, Scott B. Papp
Time and Frequency Division
National Institute of Standards and Technology
Boulder, CO, USA
E-mail: jennifer.black@nist.gov

***Summary*— We explore by design laser-wavelength conversion with integrated microresonators. Nanophotonic control of four-wave mixing in microresonators enables a new approach for laser-wavelength access, converting mature laser platforms, e.g., 1550 nm, to nearly any other wavelength band. We characterize several aspects of microresonator wavelength converters, including their tunability over >100 THz, spectral translation conversion efficiency up to 50%, and systems of microresonators that enable optical-frequency synthesis.**

Keywords—Integrated photonics, nonlinear optics, optical synthesis

Integrated nonlinear microresonators provide substantial field enhancement, which enables efficient and broadband nonlinear wavelength conversion through phase-matched four-wave mixing (FWM) [1]. Moreover, group-velocity-dispersion (GVD) engineering via tuning of the microresonator's geometric parameters controls the relevant modes involved in FWM-based nonlinear wavelength conversion processes [2]. Here, we present a versatile palette of nonlinear-wavelength-conversion processes in microresonators, including microcomb generation, optical parametric oscillation (OPO), spectral translation, and optical-frequency synthesis. We are exploring how these nonlinear processes could be applied with compact optical clocks. In this paper, we demonstrate ultrabroadband and highly efficient FWM and phase-coherent wavelength conversion. Extensions of these processes in the visible and NIR, currently under development, will support scalable infrastructure for optical clocks and quantum sensing.

Figure 1 presents several FWM-based operations of nonlinear wavelength conversion. Fig. 1a shows optical-frequency-comb, or microcomb, generation [3]. Here, a single input pump laser cascades into many microresonator modes via FWM. The pump frequency ν_0 comprises a single comb tooth and the subsequent microcomb frequencies $\nu_\mu = \nu_0 + \mu \cdot f_{rep}$ where μ is an integer and f_{rep} is the repetition rate. Octave-spanning microcombs have been realized for self-referencing, providing a phase coherent link from a microwave clock to the optical domain [4]. Targeting fewer phase-matched modes for the FWM process enables efficient OPO and spectral translation [5, 6]. Fig. 1b shows OPO in a microresonator. A single input pump frequency ν_p produces signal and idler frequencies, ν_s and ν_i, when the parametric gain overcomes the resonator losses. Below the OPO threshold, FWM-based spectral translation of light occurs for a phase-matched resonator with two input frequencies. Fig. 1c shows spectral translation of a signal frequency ν_s with an input pump ν_p. Energy conservation determines the output idler frequency $\nu_i = 2\nu_p - \nu_s$. Importantly, spectral translation can also occur from ν_i to ν_s. The conversion efficiency of optical power to other microresonator modes depends on the losses, wavelength dependent coupling, and input optical power. Moreover, by combining a microcomb with a spectral translation device, we demonstrate a system of microresonators for optical synthesis. Fig. 1d shows the system where two input frequencies, ν_0 and ν_p produce a single synthesized output frequency ν_s. The

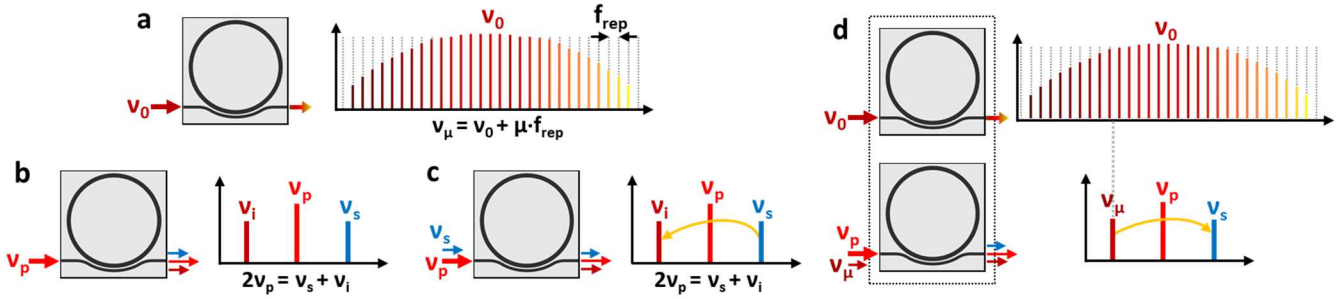

Fig. 1. a. Microcomb generation. A single pump frequency ν_p generates many frequencies ν_μ by cascaded FWM. b. OPO produces ν_s and ν_i from a single pump ν_p when the parametric gain is greater than the cavity losses. c. Spectral translation is a seeded FWM processes below OPO threshold. Two input frequencies $\nu_s(\nu_i)$ generate a new frequency $\nu_i(\nu_s)$ determined by energy conservation and provide gain on the input frequency $\nu_s(\nu_i)$. d. Combining a microcomb and spectral translation in a system of microresonators enables deterministic optical frequency synthesis by spectral translation of a comb mode ν_μ to ν_s.

microcomb generates many frequencies referenced to a microwave clock and we translate a single comb tooth ν_μ in a second microresonator to ν_s. This implements phase coherent synthesis, due to a phase lock of ν_p by optical heterodyne with the comb, ν_μ, and the energy conservation of the FWM-based spectral translation process ($2\nu_p = \nu_s + \nu_i$).

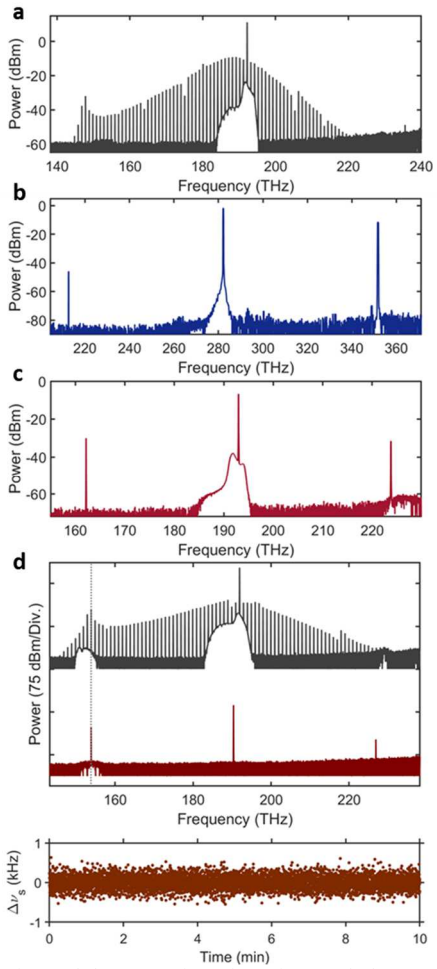

Fig. 2. Experimental demonstration of a. microcomb, b. OPO, c. spectral translation, d. optical frequency synthesis by spectral translation. d. shows the microcomb and spectral translation optical spectra offset with a dashed vertical line denoting the microcomb tooth translated to 266.901 877 622 500 THz. Bottom shows optical counter data of the synthesizer output.

We perform experiments to systematically test microcomb generation, OPO, spectral translation, and optical-frequency synthesis, using microresonators fabricated from both silicon nitride (Si_3N_4) and tantalum pentoxide (Ta_2O_5). Use of different material platforms demonstrates the fundamental requirements and advantages of phase-matching in nonlinear wavelength converters. In particular, we present soliton microcomb generation, OPOs that reach across the NIR, and a nonlinear microresonator circuit of a microcomb and a spectral translation microresonator that implements optical-frequency synthesis.

Figures 2a-c explore single nonlinear processes. Figure 2a presents a microcomb pumped in the telecom C-band at 192.2 THz and engineered for anomalous GVD. The microresonator is an SiO_2 clad Si_3N_4 ring with on-chip waveguide coupler. The microcomb spans ~90 THz (nearly 800 nm). Fig. 2b presents OPO in a Ta_2O_5 resonator with bottom SiO_2 cladding and top air cladding when pumped at 282.2 THz, yielding ν_s and ν_i at 351.8 THz and 212.6 THz. Fig. 2c presents spectral translation of light from 223.8 THz to 162.2 THz with a pump at 193.0 THz. Fig. 2a-c demonstrate that broadband geometric GVD engineering enables flexible design of laser-wavelength conversion with high efficiency across a broad spectral range. For example, the OPO spectrum in Fig. 2b yields ν_s and ν_i separated by ~140 THz and Fig. 2c demonstrates spectral translation across >60 THz.

Figure 2d presents an optical frequency synthesizer based on the nonlinear wavelength converters presented in a-c. A microcomb provides the phase coherent link from a microwave clock to the optical domain. We spectrally translate a single microcomb mode across ~70 THz to 266.901 877 622 500 THz via ν_p ~ 190.4 THz. We fully stabilize the microcomb by phase locking ν_0 and f_{rep}, and we phase lock ν_p with respect to the microcomb. We characterize the synthesizer output with a self-referenced auxiliary erbium fiber optical frequency comb with $f_{rep} = 250$ MHz. Fig. 2d presents $\Delta\nu_s = \nu - \nu_s$, which is the difference between the measured output frequency ν, measured with a frequency counter at 0.1 s gate, and the setpoint frequency, based on energy conservation $\nu_s = 2\nu_p - \nu_\mu$. We find the Alan deviation to be 22 Hz Hz in a 1 second measurement and sub-Hz accuracy over continuous 10-minute operation. We also characterize the conversion efficiency of optical power to ν_s from ν_μ as a function of pump power. We find a maximum conversion efficiency ~50% at on-chip pump power ~16 mW. At higher pump powers, parasitic OPO processes mitigate higher conversion efficiency to ν_s.

Figure 3 presents optical parametric oscillation (OPO) in tantala microresonators, corresponding to the nonlinear process diagram of Fig. 1b that converts an input pump laser to signal and idler output waves with frequency spacing $\Delta\nu = \nu_s - \nu_i$ where and are the signal and idler frequency. In essence, microresonator OPO opens up the opportunity for laser wavelength access, converting technologically mature laser platforms to wavelengths bands of interest for applications. Moreover, low additive frequency noise of the OPO process is a key advantage, and we directly measure the frequency noise spectrum of the OPO output with a high-resolution laser discriminator. These results provide insight for future research that can refine microresonator OPOs for applications, especially in the area of compact optical clocks.

We quantify microresonator OPO frequency matching using the integrated dispersion,

$$(1) \quad D_{int}(\mu) = \nu_\mu - (\nu_0 + FSR \cdot \mu),$$

where μ is the resonator mode number relative to the pump laser ($\mu = 0$), ν_μ are the μ^{th} resonator mode frequencies, and FSR is the free-spectral range at the pump. The parameter D_{int} specifically characterizes the frequency mismatch between resonator modes of equidistant mode number about the pump, particularly for the ideal OPO condition in which $D_{int}(\mu) = -D_{int}(-\mu)$. To provide wide wavelength access via OPO, we leverage a near-zero GVD regime in which slightly normal GVD phase matches four-wave mixing while mitigating competing near-pump OPO [5]. Therefore, to control

microresonator modes, i.e. $+\mu$ and $-\mu$, which are frequency matched for OPO, we exploit two mechanisms: adjustment of the pump laser mode in the 1064 nm band and adjustment of the microresonator GVD by the width of the resonator waveguide (RW) and the radius of the ring (RR). With the second mechanism, typical parameters for the microresonator include thickness of 570 nm, RR = 45 µm, and RW = 1.195 µm, which we can vary in steps as small as 2 nm. These geometric parameters directly influence D_{int} in a manner that we design, according to finite element modeling of the resonator modes based on highly accurate refractive index data for tantala thin films [7].

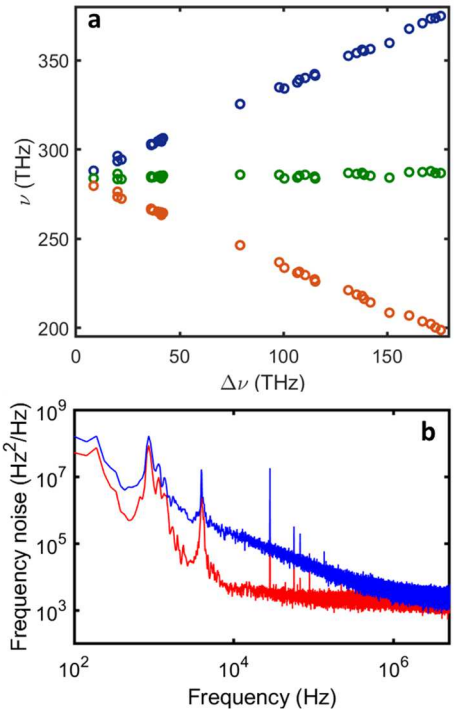

Fig. 3. a. Measured OPO frequencies, ν, vs $\Delta\nu$ for various ring geometries when pumped with a tunable 1064 nm external cavity diode laser. Maximum $\Delta\nu$ = 175.9 THz (707 nm) with ν_s=374.8 THz (800 nm) and ν_i=198.9 THz (1507 nm). b. Frequency noise for OPO pump (red; 1062 nm) and signal (blue; 1020 nm). The 1/π-linewidths for pump and signal are 28.2 kHz and 58.2 kHz, respectively.

Here we explore microresonator OPO with a pump laser wavelength in the 1064 nm band that generates signal and idler wavelength outputs spanning from 198.8 THz to 374.8 THz ($\Delta\nu = 175.9$ THz); see Fig. 3a. This makes it possible to realize laser sources designed for atomic physics experiments, for example with Rb transitions at 780 nm and 795 nm, the commensurate Cs transitions, and at 813 nm for optical lattice trapping of Sr. In the future, the opportunity exists to expand the wavelength coverage range of the OPO either through optimization of the GVD design (see below) or through nanophotonic structuring of the microresonator for direct OPO phase matching. In our experiments, we utilize an external cavity diode laser system in the 1064 nm band and an ytterbium doped fiber amplifier. We couple the pump laser to the microresonator OPO chip by use of lensed fibers and inverse taper structures at the chip edge. Our resonators exhibit typical intrinsic quality factors of $2\text{x}10^6$ and have OPO threshold power of tens of milliwatts on-chip. To initiate OPO, the pump laser can be tuned into resonance free running without the need for rapid frequency sweeping or locking. With the above context, we can understand the output tuning range of the OPO with negligible design error between out GVD modeling and experiments with fabricated tantala microresonator OPO devices. In particular, we leverage interchangeable OPO tuning through the two mechanisms described above to achieve an output range of nearly 200 THz (see Fig. 3a). We note that high resolution frequency tuning of the OPO is possible by way of temperature control of the OPO device due to tantala's thermo-optic coefficient [8].

An important characteristic of the microresonator OPO system is low additive frequency noise of the laser output beyond the pump-laser frequency noise. This behavior follows from the phase and frequency matching intrinsically required for the OPO process. Indeed, excellent common mode rejection of environmental perturbations maintains relative frequency spacing of the signal and idler with respect to the pump laser. Still, relative jitter of the pump laser and the microresonator pump mode induces frequency noise in the OPO outputs. In particular, we anticipate that laser's intrinsic frequency noise and thermorefractive noise of the microresonator [9] are the primary contributions. To explore the OPO output noise, we perform high-resolution measurements with an unbalanced optical frequency discriminator Mach–Zehnder interferometer (MZI) setup; see Fig. 3b. Here the relative imbalance of the MZI is chosen to optimize sensitivity while maintaining more than 10 MHz of Fourier frequency range to explore different noise mechanisms. The blue and red traces in Fig. 3b indicate optical frequency noise of the OPO laser and the pump laser, respectively. The pump laser features kHz level Lorentzian linewidth, enabling a sensitive test of OPO additive noise. We observe that the OPO Lorentzian linewidth is consistent with the pump laser at ~1 MHz Fourier frequency. In the close to carrier range, the OPO noise is also consistent with the pump laser noise spectrum, indicating intrinsic phase matching. Interestingly, the OPO output does exhibit enhance frequency noise in the Fourier frequency range from 1 kHz to 1 MHz. This behavior is consistent with thermodynamic fluctuations of the microresonator volume that couple to the pump mode resonance frequency due to the thermo-optic coefficient of tantala. Indeed, the decreasing power law frequency noise contribution of the device is consistent with microsecond scale thermal time constant of our microresonators with a scale of RR. The presence of thermorefractive noise in microresonator OPOs represents an interesting avenue for future experiments, especially to search for mitigation effects based on noise balance in nonlinear phase matching that have been fruitful in microresonator frequency comb systems (Fig. 1a) [10]. Still, the frequency noise spectrum of Fig. 3b is readily amendable to wideband optical frequency stabilization with respect to optical references such as high finesse, athermalized cavities and optical-frequency combs. Indeed, using the 1/π-integral

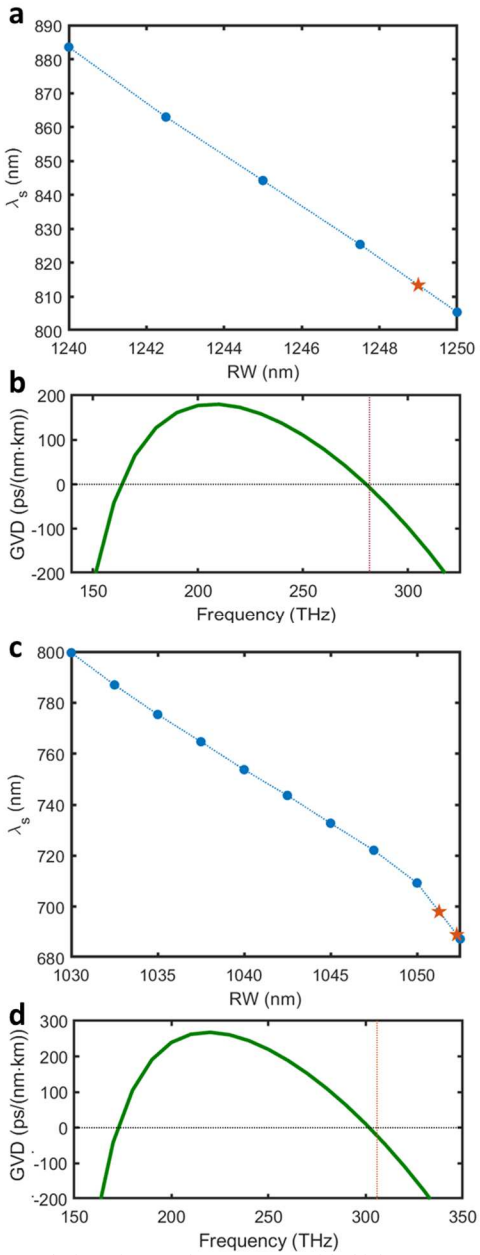

Fig. 4. OPO designs for tantala resonators with thickness 570 nm and RR = 45 um to generate relevant Sr clock wavelengths. a. Theoretical signal wavelength when pumped at 1064 nm as a function of RW. The star shows signal generation near 813 nm with RW = 1249 nm. b. The calculated GVD for the 813 nm generating device. c. Theoretical signal wavelength when pumped at 980 nm as a function of RW. Two stars at RW = 1052 nm and 1051 nm denote predicted signal generation at 689 nm and 698 nm. The GVD of the OPO device with RW = 1052 nm is plotted in d.

linewidth estimation technique in which we sum the frequency noise spectrum to accumulate $1/\pi$ phase, we assess that the OPO laser linewidth does not exceed 100 of kHz (pump and signal $1/\pi$-integral linewidth of 28.2 kHz and 58.2 kHz, respectively). This result indicates the potential of OPO tunable laser both to enable wide laser-wavelength access and to support high resolution applications in optical frequency metrology in which low residual laser frequency noise following stabilization is important.

Lastly, we present OPO designs for tantala resonators with thickness 570 nm and RR = 45 μm to generate relevant Sr clock wavelengths using commercially available tunable laser sources as seen in Figure 4. We consider GVD designs for OPO pumped at 1064 nm to target the Sr lattice wavelength near 813 nm, which is clearly possible to reach based on the experimental results in Fig 3a. Fig. 4a presents theoretical signal wavelengths generated via OPO from a pump at 1064 nm where the star denotes signal generation at 813 nm for RW = 1249 nm. The calculated GVD for the 813 nm generating devices is plotted in Fig. 4b. We also consider GVD designs for generation of 689 nm (Sr red MOT) and 698 nm (Sr clock laser) from a 980 nm pump laser. Fig 4c presents the theoretical signal wavelengths as a function of RW where the stars denote generation of 689 nm and 698 nm for RW = 1052 nm and 1051 nm, respectively. The GVD of the OPO device which generates 689 nm is plotted in Fig 4d.

In conclusion, we have demonstrated integrated nonlinear microresonators for various aspects of wavelength conversion including microcomb generation, OPO, spectral translation and optical synthesis. Due to the broadband and high conversion efficiency of the integrated nonlinear processes, these devices provide a means to deterministically convert commercialized lasers from ~ 1 μm - 1.55 μm to wavelengths across the entire near infrared.

REFERENCES

[1] Herr, T., et al. "Universal formation dynamics and noise of Kerr-frequency combs in microresonators." Nature photonics 6.7 (2012): 480-487.

[2] Black, Jennifer A., et al. "Group-velocity-dispersion engineering of tantala integrated photonics." Optics Letters 46.4 (2021): 817-820.

[3] Kippenberg, Tobias J., et al. "Dissipative Kerr solitons in optical microresonators." Science 361.6402 (2018)..

[4] Li, Qing, et al. "Stably accessing octave-spanning microresonator frequency combs in the soliton regime." Optica 4.2 (2017): 193-203.

[5] Lu, Xiyuan, et al. "Milliwatt-threshold visible–telecom optical parametric oscillation using silicon nanophotonics." Optica 6.12 (2019): 1535-1541.

[6] Lu, Xiyuan, et al. "Efficient telecom-to-visible spectral translation through ultralow power nonlinear nanophotonics." Nature Photonics 13.9 (2019): 593-601.

[7] Black, Jennifer A., et al. "Group-velocity-dispersion engineering of tantala integrated photonics," Opt. Lett., OL 46, 817–820 (2021).

[8] Jung, Hojoong, et al. "Tantala kerr nonlinear integrated photonics." Optica, OPTICA 8, 811–817 (2021).

[9] Drake, Tara, et al. "Thermal decoherence and laser cooling of Kerr microresonator solitons," Nature Photonics 14, 480–485 (2020).

[10] Stone, Jordan, et al. "Thermal and Nonlinear Dissipative-Soliton Dynamics in Kerr-Microresonator Frequency Combs," Phys. Rev. Lett. 121, 063902 (2018).